

# Engineering application of smart slope stability in-situ and remote monitoring methods in lignite opencast mine

*Z. Bednarczyk, Poltegor-Institute, Institute of Opencast Mining, Wroclaw, Poland, zbyszbed@gmail.com*

**ABSTRACT:** Slope instabilities in Polish lignite opencast mines cause problems for the effectiveness of exploitation and the environment. Its mitigation is usually difficult due to low strength parameters of clayey soils on the slopes and a high up to 300 m depth of exploitation. The paper presents the application of modern in-situ online inclinometers, PSI satellite radar interferometry, airborne and terrestrial scanning in the Belchatow opencast mine. This mine is the largest excavation in Europe a length of 13 km, a width of 3 km, and a depth of 310 m. Investigations inside the RFCS EU SLOPES project “Smarter Lignite Open Pit Engineering Solutions” were conducted by an international consortium from six European countries. In Poland research was located mainly on the west slope of the Belchatow field. In this region, the first in Polish lignite opencast mine, 100 m depth in-situ on-line inclinometer, and pore pressure monitoring system were installed at levels +42 : -58 m a.s.l. Geotechnical investigations included core drillings, laboratory index, compressibility, triaxial CIU, CID tests, numerical modeling, UAV Lidar, and terrestrial laser scanning. The total magnitude of measured in-situ ground displacements, Dec 2016 - July 2019 reached 290 mm. The largest up to 250 mm were registered, to a depth of 45 m in the direction of slope inclination, smaller up to 50 mm to a depth of 72.5 m. Displacements were accompanied by the pore pressure excess of 200 kPa. Data obtained from in-situ monitoring and laboratory tests were included in Flac numerical modeling in two cross-sections on the west slope which detected low values of stability factor  $F_s=0.83-1.14$ . In other parts of the mine and surrounding areas, satellite radar interferometry detected the largest displacement up to 60 mm/year on the external spoil dump slopes. Obtained results allowed better risk mitigation and early warning.

**Keywords:** landslide monitoring, slope stability, in-situ and remote monitoring methods, lignite opencast mines

## 1. Introduction

Human-induced natural hazards often occur in lignite opencast mines. It poses several threats due to the high size and depth of the open-pit excavations. Lignite mining still makes a significant contribution to the EU production of electricity in several European countries. In Germany, Poland, the Czech Republic, Bulgaria, Romania, and Greece 433.8 million tonnes of lignite is mined every year (Bednarczyk, Nowak 2010, Kasztelewicz 2012). That makes a significant contribution to the EU production of electricity. However, the existing mines usually operate for a long time and require exploitation of deeper and deeper deposits in open-pit excavations and storage of very large masses of overburden at spoil heaps. This causes that associated landslide risks are increasing. Mine-induced landslide losses could cause a risk for exploitation efficiency and may adversely affect the environment (Bednarczyk 2017a). The extent of landslide risk is influenced by the geological structure, soil strength parameters, land use, rainfall, changes in groundwater levels caused by the dewatering systems, the use of explosives, natural seismicity, karsts processes, seepage, and suffusion. Landslide prevention is all the more important in the mines because the scale of potential failures can be large, often counted in millions of cubic meters (Czarnecki and Organisciak 2015, Hochman 2000, Patrzyk 1996, Rybicki 1996). Landslides may pose many risks not only to the mine slope's stability but sometimes also to the adjacent areas, human life, and the environment. Prevention is difficult or even impossible, usually limited to changes in exploitation projects and slope geometry. To gain a

better understanding of the genesis of these processes, their scope, further activity, and effective counteraction, the application of complementary in-situ and laboratory research methods is of particular importance (Bednarczyk, Sandven 2004). Recognition of possible threats requires detailed knowledge of the geological structure and engineering geology conditions. These data must be identified and qualitatively characterized. Collection of geological information such as e. g. the type of soil and rock occurring in the boreholes, shear strength, the ground displacement magnitude, depth and direction, groundwater conditions, and pore pressure data is an important key to determining the instruments and parameters that should be included in the design of monitoring system. Observational methods may be used to check the size of the recorded displacements during the mine's operation and the changes in the surface area concerning those predicted earlier at the design stage. Surface displacements in large areas can be identified by modern surveying methods. Satellite data has been extensively used by the mining industry for environmental monitoring for decades (Schroeter and Gläßer 2011, Demirell et al 2011). Other methods as terrestrial or airborne laser scanning could deliver also valuable monitoring data. These types of measurements provide 3D images and allow for volume calculation using special point cloud processing software. However, in the past year's use of these techniques in Polish lignite opencast mines was relatively low. Some types of monitoring measurements allow only surface displacements measuring while another insitu is dedicated to in-place ground displacements. Very important, good-quality core drilling, combined with geophysics, laboratory tests, and numerical modeling, could provide results that are as close to the actual

conditions in the open casting as possible. For large landslides as earth flow (Cruden and Varnes 1996) due to the size of observed displacements not all of the monitoring methods could be used. The appropriate method, with its strengths and limitations, which outperform others on a given condition, could only be identified considering the local conditions and the nature of the problem (Cooper 1987, Wilkins et al 2003, Lu and Weng, 2007, Welsch et al 2000). Monitoring data implemented in numerical modeling could help in the prediction of future landslide behavior. Modeling of slope stability is possible by LEM methods based on the examination of the balance between forces and moments of forces favoring landslide-prone movement and forces opposing them at the moment of destruction. The safe state is determined by changing the geometry of the slope to a state in which the Fos value is greater than or equal to the set value. These types of methods, except for the Fos stability factor value, shall not indicate the risk associated with a given scenario (Nguyen, and Chowdhury 1984, Wu 2008). In analyses using border balance methods, the analysis is limited to the assessment of stability and does not include information on local conditions that led to landslides. Advances in soil mechanics and computer programs have made it possible to apply more comprehensive finite element FEM and SSR Shear Strength Reduction approaches. However, the open pit design in Europe is still the most common practice based on a deterministic approach. Significant progress was made to identify errors in the determination of strength parameters influencing the uncertainty of the design parameters adopted (Kulhawy 1992; Phoon and Kulhawy 1999).

In recent years in Poland is a tendency to implement the design methods adopted by Eurocode 7, taking into account the variability of geotechnical parameters (CEN 1994). The second inconvenience of the conventional approach is that the factors influencing global or partial stability factors and analysis results do not fully reliably reflect the degree of slope stability as a whole geotechnical structure (Baecher and Christian 2003; Ang and Tang 2007). According to Whitman (1984), stability ratios only indicate the possibility of failure. This may be confusing in determining the actual level of risk. Locally high stability ratios do not necessarily reflect a lower level of risk, as their performance may be negated by other doubts, weaknesses in field recognition, or an insufficient number of analyses (Christian and Ladd al. 1994). These inconveniences may pose a significant economic risk when designing. Other important not always implemented triggers are related to precipitation, changes in groundwater conditions, pore pressures in the soils, and its partial saturation caused by mine drainage and pumping dewatering systems.

Presented in the paper investigations were realized inside the EU project “Smarter Lignite Open Pit Engineering Solutions”. The project coordinated by the University of Nottingham UoN (UK) aimed at the practical implementation of modern landslide monitoring techniques and data analyses in lignite opencast mining. The project aimed to deliver new data for the design of the slopes, transport routes, and

overburden dump sites and to advance the current geotechnical technology implemented in opencast mining. Partners from UK, Czech Republic, France, Spain, and Greece analyzed the variable geotechnical conditions in selected areas using aerial, terrestrial, and in-situ monitoring techniques. Smart monitoring technologies aimed to obtain representative data that can be used for risk assessment, validation, and numerical modeling. Aerial (UAV Lidar), terrestrial (TLS), and in-situ (SAA) monitoring techniques and numerical modeling were implemented in the largest Polish lignite opencast mine.

## 2. Mine localization and geotechnical conditions.

Presented research were performed in Belchatow opencast mine in Poland. It is one of the largest open-pit excavation in Europe is located 30 km SE from the city of Lodz (Figs.1-2). The dimensions of the mine are 12.5 km in length and 3 km wide, with a current mined depth of 310 m.

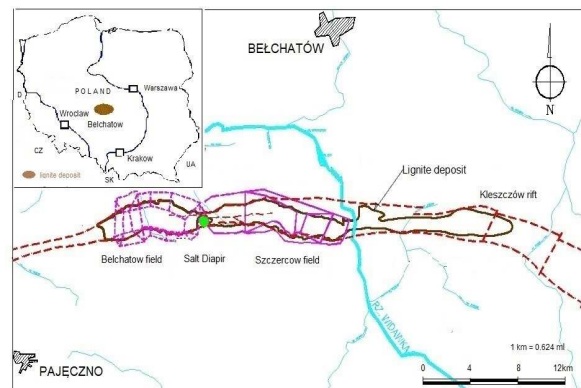


Figure 1. Localization of the Belchatow mine.



Figure 2. Belchatow Field – general view.

The exploited lignite deposit is located in the Kleszczow tectonic rift. This structural unit is formed in the Mesozoic limestone and marl bedrock as a narrow and deep tectonic unit of W-E direction filled by Neogene deposits (Fig. 3). The rift is bounded from the south and north side by large frame faults. Mesozoic Blocks inside the rift are separated along faults and dislocations. The mine leads the lignite exploitation on two operational fields, separated by a salt dome. The thickness of the Neogene deposits within the rift is over 300 m, approximately 5-15 times higher than outside it (Ciuk and Piwocki 1980). The main lignite seam is 20-

60 m thick. The largest volume of lignite is situated in deep secondary graben near the south slope of the mine. The exploitation of the Belchatow field will end in 2020, and at Szczercow field in 2038. The Belchatow field, chosen for the investigations, was affected by numerous landslide volumes of a few thousand to 3.5 mln m<sup>3</sup> with displacements from 2 mm to 2 m per day (Rybicki 1996). Low soil strength parameters of clayey overburden and over 300 m deep complex tectonic structure are causing serious geotechnical risk. Hundreds of small and large landslides volumes of hundreds or even several million cubic meters are reported there every year (Patrzyk, 1996, Rybicki, 1996; Janecki et al 1999, Jonczyk and Organisciak 2010). From 1977 to 1988, 238 landslides were reported in the mine, 80 on fixed slopes and 158 on the west exploitive slopes. Fifty percent of them had a structural nature, six percent had a shearing genesis and 44% had a complex shearing-structural genesis (Hochman 2000). In 2012, 32 risk zones on slopes were detected. Over 85% of landslides caused by mining exploitation were structural (Flisiak et al 2014). Landslide-prone structural and paleo-landslide surfaces occur at the southern slope of the pit, near deep secondary ditch structure with the greatest volume of lignite deposit. The northern slope of this mine built of Quaternary low-strength clays also posed numerous risks for conveyor belt transportation lines and power supply lines. Quaternary varved clays of unfavorable geotechnical parameters occurring on that slope often triggered a landslide. The main landslide-prone structural surfaces are contacts of Quarterly and Neogene deposits, contact of Neogene clays, and main lignite deposit. Other landslide-prone surfaces are faults, cracks, tectonic and glactectonic surfaces, low strength soils, and varved Neogene clays. A significant advantage of structural landslides is still observed as a natural consequence of the complexity of the geological structure of lignite deposit and overburden. The largest landslides occurred on the south slope of the mine along faults located at the south slope of the mine. USB1 fault is present along the entire length of the rift, while USB1a is not clear everywhere. According to Kossowski and others (1992), fault no. 1 (USB no. 1) is a narrow fault zone, constituting the upper end of a deep, concave dislocation with a W-E run associated with the Variscan period. From the north, the deposit is limited by the UNB3 fault of complementary nature to the above-mentioned above faults. In the southern part of the Kleszczow rift, there is a secondary order ditch structure. It is a narrow and deep zone limited to the south by USB1 and USB1a faults, and to the north by a fault called USB2 (Fig. 4). This ditch has a course consistent with the main direction of the rift. It is characterized by the paleo-landslide deposits prone to landslide activation an anomalous depth concerning the zone width. In recent years, due to the high depth of lignite exploitation and neighboring salt dome structure also the west slope was involved in landslide movements. Eight slope failure risk zones with active or expected landslides were reported on this t slope at the contact zone of the salt dome and the pit. This slope was selected for most of the investigations conducted inside the Polish part of the EU RFCS Slopes project.

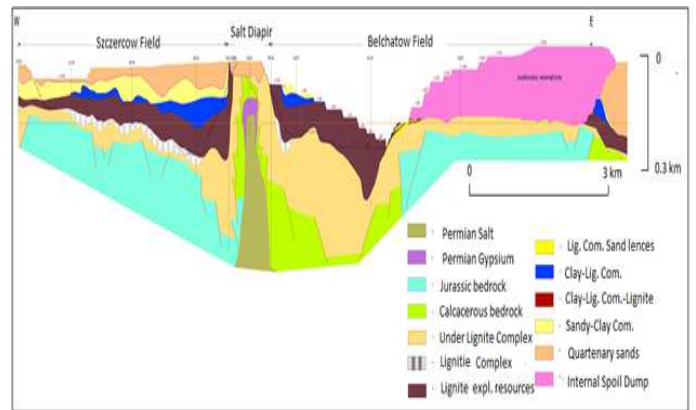


Figure 3. Geological WE cross-section of Belchatow, Szczercow field

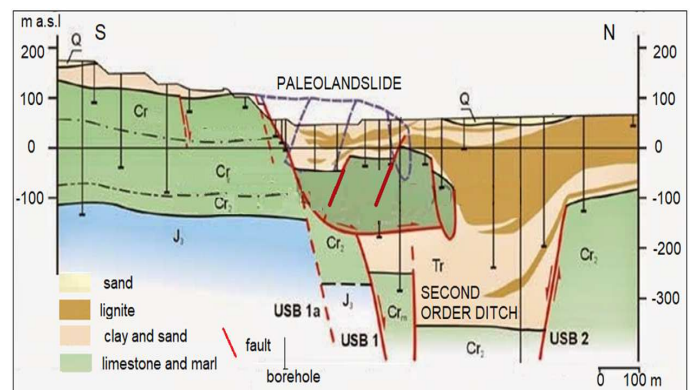
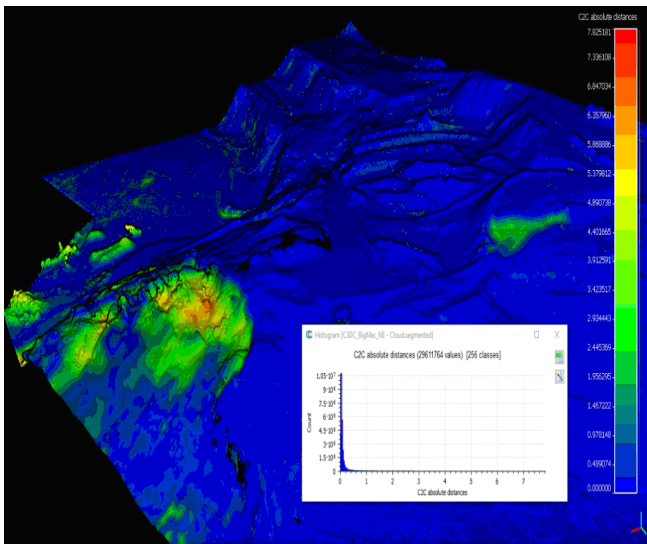


Figure 4. Cross-section of second-order ditch zone (Czarnecki and Felisiak, 2004).

### 3. LiDAR and terrestrial laser scanning

In the Slopes project, UAV LiDAR measurements were used to build a numerical terrain model in Belchatow mine using the YellowScan scanner (Figs. 5-6). The measurements were carried out in October and November 2016. For the analysis of displacements on the western slope, LiDAR airborne measurements from March 2017 were implemented. The LiDAR data sets were processed in three stages. Initially, data from the scanner were copied to a desktop computer after the flight, where point clouds were visualized and errors were identified to determine whether additional flights would be needed. After scanning, the data were processed in kinematic post-processing. In the next stage of improving data quality, measurement noise was eliminated, measurement lines were integrated, and photos were tagged into the 3D grid. This made it possible to create an orthophoto map. To calibrate the results, 11 ground-based GCP checkpoints were used. The generated point cloud of density varied from 250 to 300 points/m<sup>2</sup> and covered over 29.6 million points. The results of LiDAR scanning from a drone and aerial photographs between November 2016 and March 2017 are presented below (Fig. 5). The results indicate the occurrence of displacements and discontinuities on the western slope of the Belchatow Field. To confirm and evaluate the size of the displacements, the Cloud Compare program integrated the results of subsequent measurements. This indicated the occurrence of displacements on the western slope.



**Figure 5.** Comparison of LiDAR UAV measurements with aerial photogrammetry, displacement after three months (November 2016-March 2017) west slope of Belchatow Field, Ineris (France). source: Slopes project report Marshall et al 2019.

The displacement areas in Figure 5 are shown in green to red with corresponding displacement values estimated at approximately 6 mm. The results identify several displacement areas, including a landslide in the northern part of the western slope near the monitoring point. The obtained results recognized several displacement areas, including landslide in the northern part of the western slope near the in situ monitoring point at the level of +42 m above sea level. Terrestrial laser scanning of the western slope of the Belchatow Field was carried out in June 2016 by the University of Exeter (UK). Measurements were conducted using the Rigel-VZ4000 laser from 4 locations located on the southern slope of the Belchatow Field and two on the northern slope. A numerical terrain model was created using this data (Fig. 6). The scan results were also used to identify the slope angle and geographical direction of the slope using Arc GIS. The results of these analyses, presented in Fig. 6, indicated that the angles of inclination of individual slopes range from several to about 70 degrees.

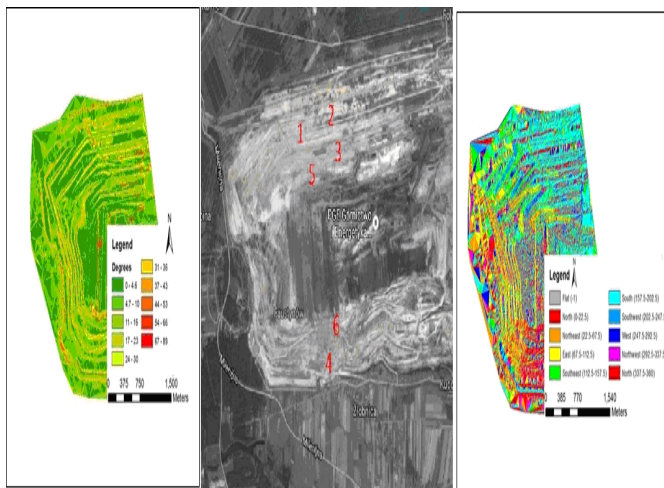


**Figure 6.** Interpretation of west slope of the Belchatow Field parameters based on TLS laser scanning, University of Exeter (UK) source: Slopes project report (Marshall et al 2019).

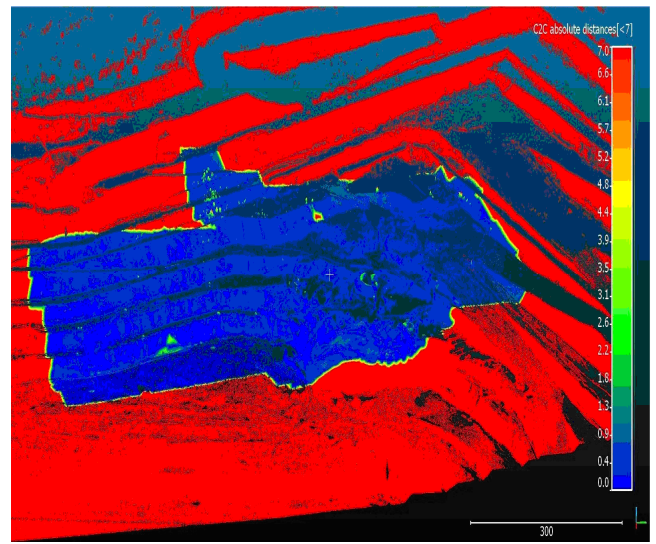


**Figure 7.** Comparison of LiDAR point cloud and the aerial image after 3-month time, ground movement (Nov 2016-March 2017) west slope of the Belchatow Field, Ineris (France). source: Slopes project report (Marshall et al 2019).

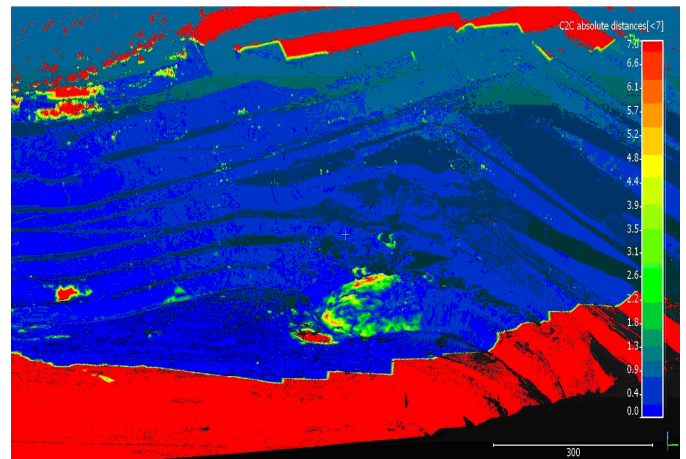


**Figure 8.** Comparison of TLS terrestrial laser scanning and the aerial photogrammetry (June 2016-March 2017) west slope of Belchatow Field, Ineris (France). source: Slopes project report (Marshall et al 2019).

To identify the landslide zones, the results of ground laser scanning TLS were also compared with the results of the later LiDAR UAV scan of November 2016 and aerial photogrammetry of March 2017 (Figs. 7-8). The models clearly show the red and green zones representing the largest displacements on a blue background representing stable areas.

#### 4. Persistent Scatterers Interferometry (PSI)

High-resolution satellite radar scanning from Cosmo SkyMed satellites (accuracy 5-10 mm) was ordered by Poltegor-Institute and performed by GAP Geophysical Applications Processing s.r.l. (Technical University Bari, Italy). The technique used for this supplementary monitoring is based on the multi-temporal SAR (Synthetic Aperture Radar) interferometry applied to COSMO-SkyMed X-Band SAR acquisitions, also known as PSI using SPINUA (Stable Points Identification in Non-Urbanized Area) software (Fig. 9). Multi-temporal SAR interferometric processing chain for in-

frastructure and ground instability monitoring software. The software enables a systematic processing strategy, capable of utilizing all archived data of a certain area, by creating a stack of differential interferograms that have a common Master image as a function of time and space. PSI techniques bypass the problem of geometrical and temporal correlation by considering temporal coherent scatterers. Furthermore, by using a large amount of data, the atmospheric signal is estimated and corrected. It offers a convenient processing framework that enables the use of all acquired images (irrespective of baseline), and a parameter estimation strategy for interferograms with low spatial coherence

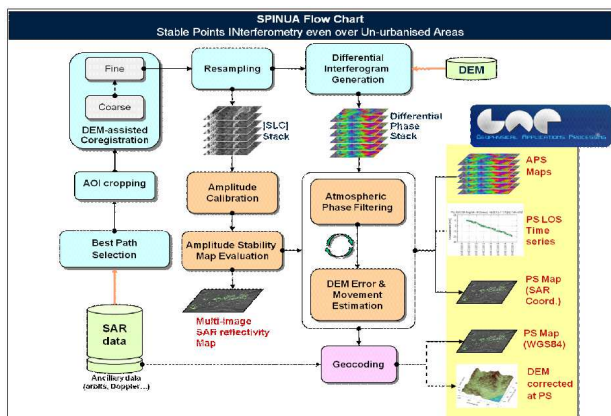


Figure 9. Flow chart of Spinua software for Persistent Scatterers Interferometry monitoring.

COSMO-SkyMed (Constellation of Small Satellites for Mediterranean basin Observation) is the largest Italian Space Systems for Earth Observation. The system consists of a constellation of four Low Earth Orbit mid-sized satellites with the nominal orbit configuration presented in Figures 10-11. Each satellite is equipped with a multi-mode high-resolution Synthetic Aperture Radar (SAR) operating at X-band, deployed with a staggered policy: all the four satellites of the COSMO-SkyMed constellation are currently in orbit and operational. The ten-fold increase of the ground range resolution (concerning ERS/ENVISAT/Sentinel-1 data) and the shorter orbital repeat cycle (16 days for the single satellite of the COSMO-SkyMed constellation, only 4 days for the full COSMO-SkyMed constellation) first ESA missions (35 days for ERS/ENVISAT) has contributed to open completely innovative investigation realms, contributing to improved monitoring capabilities of space-borne remote sensing instruments.

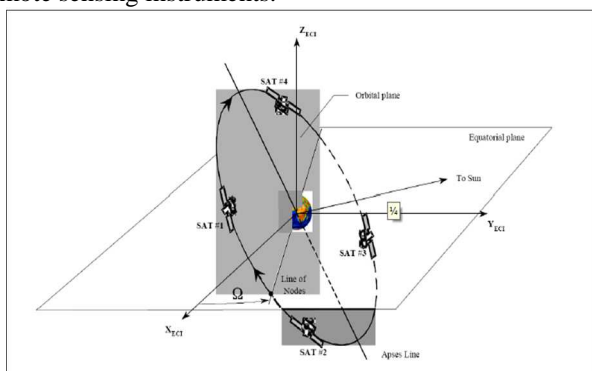


Figure 10. COSMO-SkyMed nominal orbit configuration

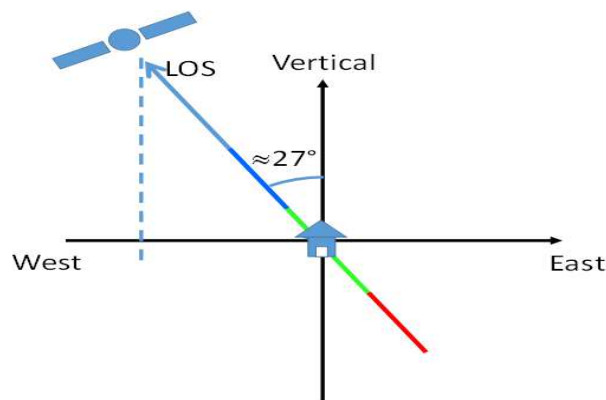


Figure 11. Acquisition geometry and line of sight of the COSMO-SkyMed images processed in the present work. Note the use of blue color for movements towards the satellite and the use of red color for movements away from the satellite.

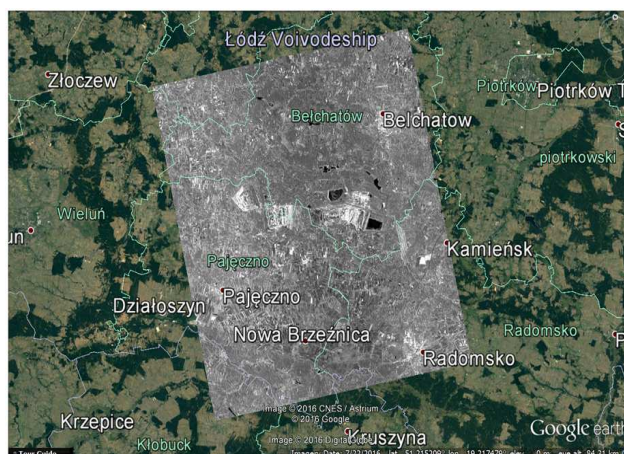


Figure 12. Area covered by the COSMO-SkyMed satellite photo acquisitions.

The COSMO-SkyMed SAR instrument was being operated STRIPMAP mode achieving medium resolution, medium swath imaging with two radar in ascending geometry with a spatial resolution of 3 meters. The preliminary results consist of a displacement map in kml provided only the average displacement velocity of the PS identified over the scene. Although the preliminary processing worked on a decimated number of PS, it was able to find 100.000 PS (e.g. reliable measurement points) over the Belchatow mine and nearby area (appr. 1600 km<sup>2</sup>) reporting displacements velocities (Fig. 12). PS velocities are relative to the satellite position: positive values (blue points) correspond to points moving toward the satellite, whereas negative values (red points) correspond to points moving away from the satellite. Points moving orthogonally to the line of sight are “seen” as motionless points by the satellite. A detailed view of the map over the Belchatow mine that is produced with different color bars to better illustrate the entity of the displacements (Fig. 13). More specifically, it is possible to detect that the largest subsidence (red color) occurred on external spoil dump storage in Szczercow, internal spoil dump and internal storage of ashes from the power plant. The largest uplift – probable changes of the slope morphology (blue color) connected with landslide movements occurred at the north and south slope of Belchatow Field. By using the color bar saturated to 50 mm a year, it is possible to infer that

the largest subsidence (red color) occurred on external Szczercow spoil dump and upper part of the internal spoil dump. By using the color bar saturated to 100 mm a year it is possible to infer these areas (red dots) were limited to external Szczercow spoil dump. Using CosmoSkyMed satellite photographs, identified 781206 points for which displacement was determined. In total, eighteen displacement zones were identified in the external overburden spoil dump in Szczercow and some other regions including the slopes of the Belchatow and Szczercow pits. The highest settlements up to 60 mm/year were found on the eastern slope of the external overburden spoil dump in Szczercow. On the western slope of this spoil heap, the settlement was 30-40 mm per year. In the area of the southern slope of the Belchatow Field, the displacements (comparable points) were 19-24 mm/year, whereas in the area of the western slope from 9.5-10 mm/year. These measurements enabled a very detailed analysis of displacements in a large area. It should be noted that the method allows examining displacement initiating larger landslides and their further development. However, this method has also limitations related to places where the morphology changes very quickly and does not allow for comparison of the same elements of the terrain. This is the case in places where the displacements and changes of terrain surface are very quick and may amount to e.g. up to 1000 mm / day, as for newly stored spoil dump soils (when the morphology of dumping soil changes very quickly, it is no data in such a places - white color in the plots). A similar situation with a lack of data could be observed on very active landslides with high displacements, rapidly changing its morphology (e.g. landslide on the southern slope of the Belchatow Field). In such cases, permanently installed reflectors on the slope surface could help in measurements (until the time of fall down or destruction of special reflectors).

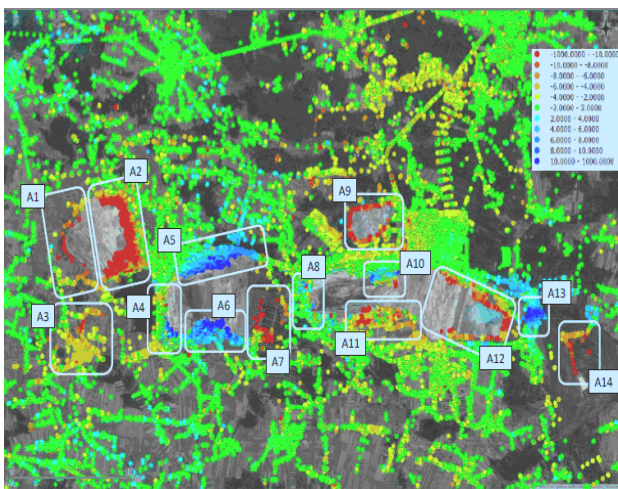


Figure 13. Results of Persistent Scatter Interferometers (PSI).

## 5. In-situ monitoring instrumentation and laboratory tests

The in-situ online continuous monitoring system was installed in December 2016 at the level +42.6 m a.s.l. in the pit, 210 m, below the natural terrain level (Figs. 15-20). It was located in the northern part of the west slope

of the Belchatow field in the IVW risk area in the NE contact zone of the salt dome (Fig. 20). The installation of a 100 m depth monitoring system in a 132 mm borehole required a detailed geological description of soil type, moisture content, consistency, and field tests of the soil strength parameter (Fig. 14). For recognition of soil index and strength parameters, 31 undisturbed samples diameter of 90 mm, length of 500-700 mm were collected. Initial identification of index strength parameters was based on 36 field penetrometer and vane shear strength tests performed on the soil samples from the borehole. The results indicated cohesion ( $C_u$ ) 24-44.7 kPa and undrained shear strength 23.9-47.8 kPa. The lowest values of strength parameters were recognized for silty clays at 54 m depth, the highest in clay with lignite at 29.5 m depth. Laboratory tests program included an index, direct shear, IL oedometer compressibility, triaxial CIU, and CID tests. Index tests covered grain size, moisture content, unit weight, dry unit weight analysis. Tests included also the content of organic material and Attenberg limits.

Polskiej Instytut Wrocław, Parkowa 25, Poland		Borehole Geological Profile Profile number r 1726B B/IN 13W						Brd No.1 Drilling rig: USB-30	
Place: Rogawiec Commune: Kiszczaw County: Belchatow Province: Lodzkie		Object: inclinometer installation 1726B B/IN 13W Investor: KMB Belchatow Drilling contractor: ALGEO, Grabowia Straszyn Geological supervision: Dr Zdzisław Boharzyk				Drilling system: core/programm/day Ground level: 42.00 m a.s.l. Scale 1:500 Drilling date: 2016-12-12			
Profile	Depth [m]	Geological description	Soil type	Consistency	Moisture	Consistency	Soil strength	Soil strength	
1	2	3	4	5	6	7	8	9	
	0.00	0.20 brown oad, lignite, brown	Cs	c1	dry	CL			
	0.20	0.50 silty clay, brown	C	c1	moist	CL			
	0.50	1.00 clay, brown	C	c1	moist	CL			
	1.00	1.50 clay, brown	C	c1	moist	CL			
	1.50	2.00 brown oad, lignite, brown	L	1	moist	-			
	2.00	2.50 brown oad, lignite, brown	L	1	moist	-			
	2.50	3.00 brown oad, lignite, brown	L	1	moist	-			
	3.00	3.50 brown oad, lignite, brown	L	1	moist	-			
	3.50	4.00 brown oad, lignite, brown	L	1	moist	-			
	4.00	4.50 brown oad, lignite, brown	L	1	moist	-			
	4.50	5.00 brown oad, lignite, brown	L	1	moist	-			
	5.00	5.50 brown oad, lignite, brown	L	1	moist	-			
	5.50	6.00 brown oad, lignite, brown	L	1	moist	-			
	6.00	6.50 brown oad, lignite, brown	L	1	moist	-			
	6.50	7.00 brown oad, lignite, brown	L	1	moist	-			
	7.00	7.50 brown oad, lignite, brown	L	1	moist	-			
	7.50	8.00 brown oad, lignite, brown	L	1	moist	-			
	8.00	8.50 brown oad, lignite, brown	L	1	moist	-			
	8.50	9.00 brown oad, lignite, brown	L	1	moist	-			
	9.00	9.50 brown oad, lignite, brown	L	1	moist	-			
	9.50	10.00 brown oad, lignite, brown	L	1	moist	-			
	10.00	10.50 brown oad, lignite, brown	L	1	moist	-			
	10.50	11.00 brown oad, lignite, brown	L	1	moist	-			
	11.00	11.50 brown oad, lignite, brown	L	1	moist	-			
	11.50	12.00 brown oad, lignite, brown	L	1	moist	-			
	12.00	12.50 brown oad, lignite, brown	L	1	moist	-			
	12.50	13.00 brown oad, lignite, brown	L	1	moist	-			
	13.00	13.50 brown oad, lignite, brown	L	1	moist	-			
	13.50	14.00 brown oad, lignite, brown	L	1	moist	-			
	14.00	14.50 brown oad, lignite, brown	L	1	moist	-			
	14.50	15.00 brown oad, lignite, brown	L	1	moist	-			
	15.00	15.50 brown oad, lignite, brown	L	1	moist	-			
	15.50	16.00 brown oad, lignite, brown	L	1	moist	-			
	16.00	16.50 brown oad, lignite, brown	L	1	moist	-			
	16.50	17.00 brown oad, lignite, brown	L	1	moist	-			
	17.00	17.50 brown oad, lignite, brown	L	1	moist	-			
	17.50	18.00 brown oad, lignite, brown	L	1	moist	-			
	18.00	18.50 brown oad, lignite, brown	L	1	moist	-			
	18.50	19.00 brown oad, lignite, brown	L	1	moist	-			
	19.00	19.50 brown oad, lignite, brown	L	1	moist	-			
	19.50	20.00 brown oad, lignite, brown	L	1	moist	-			
	20.00	20.50 brown oad, lignite, brown	L	1	moist	-			
	20.50	21.00 brown oad, lignite, brown	L	1	moist	-			
	21.00	21.50 brown oad, lignite, brown	L	1	moist	-			
	21.50	22.00 brown oad, lignite, brown	L	1	moist	-			
	22.00	22.50 brown oad, lignite, brown	L	1	moist	-			
	22.50	23.00 brown oad, lignite, brown	L	1	moist	-			
	23.00	23.50 brown oad, lignite, brown	L	1	moist	-			
	23.50	24.00 brown oad, lignite, brown	L	1	moist	-			
	24.00	24.50 brown oad, lignite, brown	L	1	moist	-			
	24.50	25.00 brown oad, lignite, brown	L	1	moist	-			
	25.00	25.50 brown oad, lignite, brown	L	1	moist	-			
	25.50	26.00 brown oad, lignite, brown	L	1	moist	-			
	26.00	26.50 brown oad, lignite, brown	L	1	moist	-			
	26.50	27.00 brown oad, lignite, brown	L	1	moist	-			
	27.00	27.50 brown oad, lignite, brown	L	1	moist	-			
	27.50	28.00 brown oad, lignite, brown	L	1	moist	-			
	28.00	28.50 brown oad, lignite, brown	L	1	moist	-			
	28.50	29.00 brown oad, lignite, brown	L	1	moist	-			
	29.00	29.50 brown oad, lignite, brown	L	1	moist	-			
	29.50	30.00 brown oad, lignite, brown	L	1	moist	-			
	30.00	30.50 brown oad, lignite, brown	L	1	moist	-			
	30.50	31.00 brown oad, lignite, brown	L	1	moist	-			
	31.00	31.50 brown oad, lignite, brown	L	1	moist	-			
	31.50	32.00 brown oad, lignite, brown	L	1	moist	-			
	32.00	32.50 brown oad, lignite, brown	L	1	moist	-			
	32.50	33.00 brown oad, lignite, brown	L	1	moist	-			
	33.00	33.50 brown oad, lignite, brown	L	1	moist	-			
	33.50	34.00 brown oad, lignite, brown	L	1	moist	-			
	34.00	34.50 brown oad, lignite, brown	L	1	moist	-			
	34.50	35.00 brown oad, lignite, brown	L	1	moist	-			
	35.00	35.50 brown oad, lignite, brown	L	1	moist	-			
	35.50	36.00 brown oad, lignite, brown	L	1	moist	-			
	36.00	36.50 brown oad, lignite, brown	L	1	moist	-			
	36.50	37.00 brown oad, lignite, brown	L	1	moist	-			
	37.00	37.50 brown oad, lignite, brown	L	1	moist	-			
	37.50	38.00 brown oad, lignite, brown	L	1	moist	-			
	38.00	38.50 brown oad, lignite, brown	L	1	moist	-			
	38.50	39.00 brown oad, lignite, brown	L	1	moist	-			
	39.00	39.50 brown oad, lignite, brown	L	1	moist	-			
	39.50	40.00 brown oad, lignite, brown	L	1	moist	-			
	40.00	40.50 brown oad, lignite, brown	L	1	moist	-			
	40.50	41.00 brown oad, lignite, brown	L	1	moist	-			
	41.00	41.50 brown oad, lignite, brown	L	1	moist	-			
	41.50	42.00 brown oad, lignite, brown	L	1	moist	-			
	42.00	42.50 brown oad, lignite, brown	L	1	moist	-			
	42.50	43.00 brown oad, lignite, brown	L	1	moist	-			
	43.00	43.50 brown oad, lignite, brown	L	1	moist	-			
	43.50	44.00 brown oad, lignite, brown	L	1	moist	-			
	44.00	44.50 brown oad, lignite, brown	L	1	moist	-			
	44.50	45.00 brown oad, lignite, brown	L	1	moist	-			
	45.00	45.50 brown oad, lignite, brown	L	1	moist	-			
	45.50	46.00 brown oad, lignite, brown	L	1	moist	-			
	46.00	46.50 brown oad, lignite, brown	L	1	moist	-			
	46.50	47.00 brown oad, lignite, brown	L	1	moist	-			
	47.00	47.50 brown oad, lignite, brown	L	1	moist	-			
	47.50	48.00 brown oad, lignite, brown	L	1	moist	-			
	48.00	48.50 brown oad, lignite, brown	L	1	moist	-			
	48.50	49.00 brown oad, lignite, brown	L	1	moist	-			
	49.00	49.50 brown oad, lignite, brown	L	1	moist	-			
	49.50	50.00 brown oad, lignite, brown	L	1	moist	-			
	50.00	50.50 brown oad, lignite, brown	L	1	moist	-			
	50.50	51.00 brown oad, lignite, brown	L	1	moist	-			
	51.00	51.50 brown oad, lignite, brown	L	1	moist	-			
	51.50	52.00 brown oad, lignite, brown	L	1	moist	-			
	52.00	52.50 brown oad, lignite, brown	L	1	moist	-			
	52.50	53.00 brown oad, lignite, brown	L	1	moist	-			
	53.00	53.50 brown oad, lignite, brown	L	1	moist	-			
	53.50	54.00 brown oad, lignite, brown	L	1	moist	-			
	54.00	54.50 brown oad, lignite, brown	L	1	moist	-			
	54.50	55.00 brown oad, lignite, brown	L	1	moist	-			
	55.00	55.50 brown oad, lignite, brown	L	1	moist	-			
	55.50	56.00 brown oad, lignite, brown	L	1	moist	-			
	56.00	56.50 brown oad, lignite, brown	L	1	moist	-			
	56.50	57.00 brown oad, lignite, brown	L	1	moist	-			
	57.00	57.50 brown oad, lignite, brown	L	1	moist	-			
	57.50	58.00 brown oad, lignite, brown	L	1	moist	-			
	58.00	58.50 brown oad, lignite, brown	L	1	moist	-			
	58.50	59.00 brown oad, lignite, brown	L	1	moist	-			
	59.00	59.50 brown oad, lignite, brown	L	1	moist	-			
	59.50	60.00 brown oad, lignite, brown	L	1	moist	-			
	60.00	60.50 brown oad, lignite, brown	L	1	moist	-			
	60.50	61.00 brown oad, lignite, brown	L	1	moist	-			
	61.00	61.50 brown oad, lignite, brown	L	1	moist	-			
	61.50	62.00 brown oad, lignite, brown	L	1	moist	-			
	62.00	62.50 brown oad, lignite, brown	L	1	moist	-			
	62.50	63.00 brown oad, lignite, brown	L	1	moist	-			
	63.00	63.50 brown oad, lignite, brown	L	1	moist	-			
	63.50	64.00 brown oad, lignite, brown	L	1	moist	-			
	64.00	64.50 brown oad, lignite, brown	L	1	moist	-			
	64.50	65.00 brown oad, lignite, brown	L	1	moist	-			
	65.00	65.50 brown oad, lignite, brown	L	1	moist	-			
	65.50	66.00 brown oad, lignite, brown	L	1	moist	-			
	66.00	66.50 brown oad, lignite, brown	L	1	moist	-			
	66.50	67.00 brown oad, lignite, brown	L	1	moist	-			
	67.00	67.50 brown oad, lignite, brown	L	1	moist	-			
	67.50	68.00 brown oad, lignite, brown	L	1	moist	-			
	68.00	68.50 brown oad, lignite							

**Table 1.** The results of triaxial tests

No	Depth [m]	Soil type	Test type	Soil strength parameters			
				Friction angle		Cohesion	
				$\phi$ [deg]	$\phi'$ [deg]	c [kPa]	c' [kPa]
1	4.0	loamy sand	CIU	42.9	42.9	0.0	0.0
2	16.4	sandy silt	CIU	33.5	34.1	27.8	19.7
3	29.3	loam	CIU	11.4	14.5	66.3	103.2
4	33.0	silty clay	CIU	21.8	30.3	129.2	32.5
5	33.5	lignite	CID		19.0		200.0
6	46.4	clay	CIU	8.5	9.8	6.3	18.7
7	47.5	loamy sand	CIU	55.1	28.6	0.0	0.0
8	50.5	clay	CIU	12.9	15.5	373.0	345.1
9	57.5	loamy sand	CIU	29.1	28.4	0.0	0.0
10	81.0	sandy silt	CIU	35.3	34.9	32.3	41.2
11	81.5	sandy silt	CIU	32.3	32.4	154.9	153.6

The triaxial tests were performed on 30 soil specimens taken from the borehole for online monitoring installation. It included one CIU and eleven CID tests. Test procedure required tests at least 2-3 soil samples, with initial consolidation and saturation in steps (with control of B-pore pressure parameter). Consolidation pressure was increased to 50, 100, 200, 400, 800 kPa depending on the specimen depth. Usually, consolidation lasts at least 24 hours until no significant changes in specimen volume were observed. Shearing was performed with a low speed of 0.025 mm/s to avoid high pore pressure during the shearing stage. Specimens' diameter of 50 mm and 100 mm height was prepared carefully. However, many lignite and clay specimens were damaged and disintegrated during cutting. Other types of difficulties were connected with the extraction of undisturbed NNS specimens from Osterberg stainless steel cylinders. These problems were caused by the stiff and cracked character of lignite deposits and their heavy OCR. The volume of soil specimens was increasing during the extraction from the stainless steel tubes. Specimens are often separated into small parts. In many cases form of cylindrical specimens for tests impossible. Undisturbed samples from Osterberg cylinders disintegrated during the extraction. Most of the samples for triaxial tests were cut from the drilling core protected in plastic tubes. The structure of lignite samples and numerous cracks in the same causes damage also the rubber membrane during the consolidation phase. All these factors made interpretation of the triaxial test and characterization of strength parameters of soil layers difficult. The interpretation of triaxial test results included plots of deviator stress, total, effective stress path plots, and Mohr-Coulomb circles. The obtained strength parameters are presented in Table 2. It presents the calculation of strength parameters using the Mohr-Coulomb Criterion for eleven triaxial tests. The lowest strength parameters were recognized in clay 46.4-47.4 m depth. The highest in lignite 33.5-34.0 m depth and silty clay 33.0-33.5 m depth. However, in some cases, it was not enough tests for comprehensive characterization, for the

same type of soils only one test (2-3 specimens) due to the impossibility of extraction of specimens from the Osterberg sampler. Some tests were interrupted or failed due to membrane damage, lack of power supply, or difficulties connected with the forming of specimens (tests No 1, 9-13, 15).

The monitoring instrumentation included two hundred 3D displacements sensors located every 0.5 m, 3 magnetometers for control of rotation and ground temperature sensors every 4 meters. The continuous inclinometer SAA system is 100 m depth, built from rigid segments. Segments could be tilted in any direction but not twisted. One segment is 0.5 m length. One segment includes 3 tilt sensors measuring range  $\pm 45$  degrees, accuracy 0.02 mm/m, the mistake of joints  $\pm 0.250$ . Every octet (4 segments) is equipped with a ground temperature sensor for the correction of temperature effects. The maximum range of equipment depends on the speed and depth of movements (usually not more than 500 mm). The system is waterproof up to 980 kPa. System powered by a solar panel was additionally equipped with a VW pore pressure sensor located at a depth of 30 m. The GPRS data are registered every 6 hours and available online from 19 December 2016 till now. Data were recorded every 6 hours. Connection with field station was realized every day between 11 AM-1 PM. Recorded data were interpreted and analyzed in SAA3D software as plots of magnitude, cumulative, incremental displacements and pore pressure plots (Figs. 16-18). For an early warning, the limit of 30 mm per day was selected in the software.

**Figure 15.** The on-line monitoring station in Belchatow mine.

All obtained data were sent every two weeks to the Belchatow Mine (PGE Company) as reports with the description of observed trends, analysis, and conclusions. The Slopes project was ended in May 2018 but the system is still operating. Till the end of July 2019, the highest displacements were recorded at depth of 35 m, at level + 7 m a.s.l (Fig. 16). In the direction of slope inclination (x) the highest displacements up to 250 mm were recorded at depths of 0-45 m. In the perpendicular direction (y) displacements up to 50 mm were recorded to a depth of 70 m. The total resultant vector of displacements was 290 mm (Fig. 17). The highest displacements of 80 mm were observed in the period June-July 2018. High displacements were also observed in the period February - April 2019, when they increased by 70 mm, February 2017, 60 mm and August - Sep-



## 6. Numerical modeling

The stability analyses of the west slope were performed in two cross-sections (Fig. 20). Due to the complex geological structure, they required generalization of the introduced model of the western slope of the quarry. For this purpose, 9 layers with similar strength parameters were separated. The interpretation of the derived design values of effective strength was based on the Eurocode 7 recommendations (PN EN 1997-1:2008, PN-EN 1997-2:2009) based on the so-called comparable experience. The strength parameters used for calculations were taken from 30 indexes and CIU triaxial laboratory tests and based on corrected values from previous tests and modeling (Poltegor-Projekt 2002, Bednarczyk 2017b) and are presented in Tab 4. The correction method for effective calculation parameters were estimated using previous assessments and methods (Hawrysz 2013, Phoon, Kulhawy 1999). In the case of Mesozoic rocks, the parameters were determined using the GSI classification (Marinos, Hoek 2005). The exemplar geometry of the separated layers is shown in Figure 21.

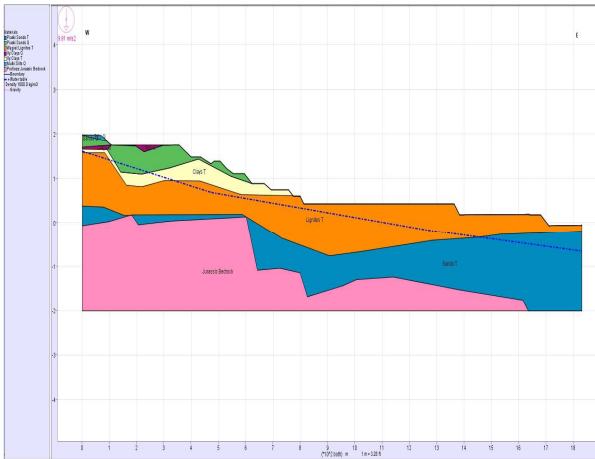


**Figure 22.** Slope stability analysis 20WE, SSR Method, geotechnical layers.

The analyses of slope stability at the west slope of the mine were performed using Flac 8.0 codes. The Shear Strength Reduction Method tends to reflect the actual condition on the slopes leading to the reduction of shear strength of soil till to stage of losing stability. The software allows the implementation of the boundary condition using various soil and rock models, different load, and groundwater conditions. The implemented Mohr-Coulomb elastoplastic strength model required specification of bulk density, effective cohesion, and effective angle of internal friction. Slope stability was analyzed with Flac 8.0 2D in two cross-sections 18WE and 20WE in the highest gradient lines. The calculation grid had dimensions of 1×1 m and included 50.000 calculation steps. The applied constitutive model of linear-elastic soil contained an approximate depth of the groundwater table. The results of modeling indicate a high risk of landslide on the western slope. This is confirmed by field observations and monitoring (Figs. 16-19, 21). It should be added that the analyses are approximate as they do not take into account the influence of salt structure. This was caused by the

relatively large distance from the landfill (in the scale of calculation grid for the slope) and the lack of representative data for the landfill for calculations.

**Table 2.** Strength parameters implemented in the numerical analysis.

No	Soil/rock type	$\rho$	c [kPa]	$\phi$ [°]
1	Sand (Q)	18.5	1.0	30.0
2	Glacial loam (Q)	21.8	40.0	9.2
3	Silt (Q)	21.3	40.0	15.0
4	Clay (Q)	20.8	80.0	5.3
5	Clay (N)	21.1	89.0	5.8
6	Lignite (N)	11.8	170.0	14.8
7	Sands (N)	19.5	1.0	32.0
8	Mesozoic rock (M)	25.0	338.0	27.1

The SSR method is effective in terms of the detection of the weakest zones of the analyzed slopes. It allowed prediction of the relative factor of safety Fs with higher precision than the limit equilibrium method analyzing the most probable circular slip surface. This way stress/strain relationship, tangential strain rate, shear strain rate contours [s-1], maximum velocity vectors [m/s] were calculated. These allowed the initial prediction of slip surface, the zones of occurrence of the greatest deformation, and the velocity of movements within the analyzed slopes.

The stability coefficients obtained in the Flac program were unfavorable and ranged from 0.85 in section 18 WE (near a landslide) to 1.14 in section 20 WE (Figs. 22-24). In complex geological-engineering conditions, the reliability of numerical modeling may depend on many factors related to the uncertainty of calculation parameters, simplified geometric model, strength parameters introduced, length of analyzed cross-sections, and the applied calculation grid. The analyses of western slope stability were also performed with the LEM border equilibrium methods using the Bishop and Janbu methods (Fig. 25). The results of all the analyses are presented in Table 3. The result of the local analysis and the field inspection indicates that it is a high landslide risk on the west slope of the mine (Fig. 27). The movements were caused by multiple factors as mining influence, the slope height and strength parameters, and salt dome influence. The salt structure influence was not included in these preliminary local analyses due to the relatively high distance to the salt dome and lack of representative data but it should be implemented in future analysis. It should take into account the rheological properties of salt in the salt dome and surrounding layers. However, in such complex geotechnical conditions, its credibility depends on several factors. The errors of interpretation may be of a different origin. These are usually associated with the uncertainty of calculation parameters and the simplified geometric model. Errors can arise mainly from the approximations of geometrical models for the analysis, usage of simplified strength parameters, length of the analyzed cross-sections, and applied computing grid.



Figure 23. Slope stability analysis 20WE, SSR method, Fos = 1.14.

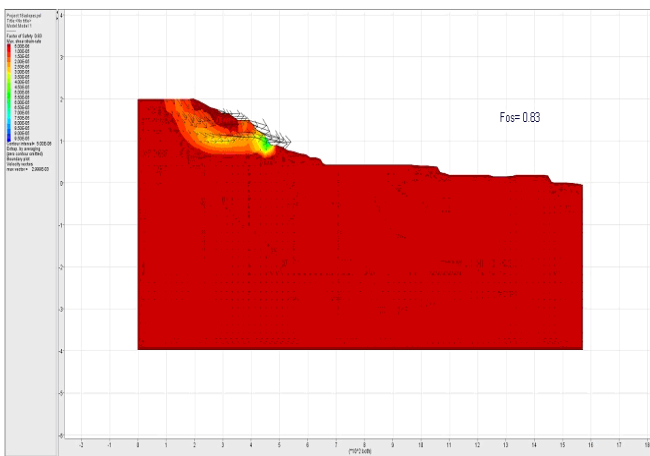


Figure 24. Slope stability analysis, 18 WE, SSR method, 20WE, Fos= 0.83.

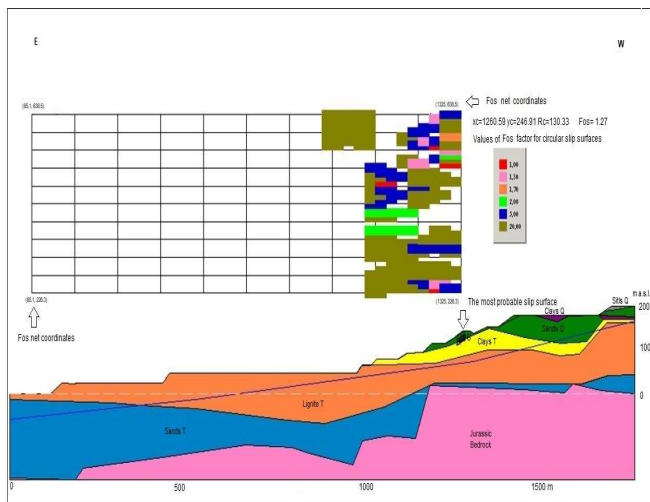


Figure 25. Slope stability analysis, 20WE, LEM Janbu Method, Fos = 1,27.

Table 3. Results of slope stability analysis at the western slope of the Belchatow Field.

Method	Fos cross-section 20 WE	Fos cross-section 18 WE
SSR Flac	0.83	1.14
LEM Bishop	1.34	1.16
LEM Janbu	1.46	1.27

The west slope and its near surroundings are subjected to a very complex state of stresses in the rift. Significant changes in the stresses at the slopes due to mining and influence of salt dome can be the cause of landslide processes, consisting of significant deformations, stress relaxation, an opening of natural cracks and water infiltration and change of water flow conditions. Large changes in the stress conditions may cause the re-activation of faults, tectonic surfaces and cracks, and trigger ground movements at the west slope. The analysis didn't include decreased geotechnical parameters at surfaces favorable for landslides activations, for example, Quaternary / Neogene contacts, paleolandslides slip surfaces, etc. The introduction of these surfaces and associated low values of strength parameters may also adversely affect the value of Fos.



Figure 26. Landslide near the cross-section 20 WE, west slope of the Belchatow field.

## 7. Conclusions

In-situ and remote monitoring and modeling methods were implemented in Belchatow lignite opencast mine. The results of the monitoring provided new displacement, pore pressure, and slope stability data. These data could be used to control the displacements during the exploitation concerning those predicted at the design stage.

Displacements at large areas around the mine were investigated using PSI measurements. Its analyses detected that the PSI method had limitations for high rates of displacements. Quick and reliable data for individual slopes was acquired using aerial LiDAR UAV scans and terrestrial laser scanning. All these data had great potential however it should be carefully calibrated by standard geodesy reference points.

In-situ inclinometer measurements detected displacements of 290 mm to a depth of 46 m (level +40 to -6 m a.s.l.) in over 2.5 year time (930 days).

The surface displacements interpreted from PSI measurements were different from those interpreted from in-situ measurements because they have the same limitations connected with its high range and with the direction of satellite movement. Limitations for PSI were particularly visible in landslide areas where the size of movements was very high and spoil dumps where the morphology was changing very fast. Besides these limitations, the PSI measurements were very beneficial for the early detection of landslide initiation and delivered many valuable data for large areas. Displacement observed using the PSI method varied 19-20 mm in 2 years.

Aerial UAV LiDAR scanning tested by Slopes project partners at this area estimated surface displacements at the west slope at 7 mm in 3 months (between the measurements). Comparison of results from different monitoring methods confirmed differences between surface displacement, which is good for large areas, and ground displacement, which can detect small ground displacements earlier and more accurately. These small movements usually preceding large landslides in the most endangered areas. Conventional inclinometers usually measure ground displacement up to 110 mm and may not be proper at larger ranges. It should also be noted that not every laser scanner will be suitable for slopes scanned from a distance of approximately 3 km, which was required in the case of the Belchatow mine.

Continuous SAA monitoring system supplied with magnetometers could measure the much higher size of displacements up to 500 mm. Implemented methods should always be adjusted to the type and magnitude of the displacements. In areas of high movements counted in meters installation of in-situ instrumentation could be useless and not effective. Airborne scanning systems could have better possibilities. They enabled the quick acquisition of various monitoring data even in the conditions of large movements. Additionally, this type of point cloud data can be used to determine layers within the slopes, the location of the geological structures, faults, and discontinuities. These data should be always carefully calibrated by standard geodesy reference points. All aerial or satellite measurements should be unified in scale and when it is possible compared with inclinometer ground measurements. The investigated slope was characterized by a low stability factor  $Fos = 0.83-1.10$ .

The in-situ monitoring checked the stability of the western slope. In other areas of the mine, satellite radar PSI interferometry allowed for the separation of 18 zones with increased displacements. Full elimination of landslide hazards in opencast lignite mines is not possible. Knowledge of past processes, experience from the implementation of new research methods inside the Slopes project should contribute to better identification of risks and the selection of optimal mitigation measures. In areas particularly vulnerable to landsliding, it may be useful to develop individual methods for remote monitoring and detailed procedures for interpretation of movement's size, depth, and direction. It should be

stressed, however, that forecasting the occurrence of landslides in Polish opencast lignite mines is usually very complex. Implementation of presented methods should benefit the mitigation measures.

## Acknowledgment

The Slopes RFCR-CT-2015-00001 Project presented in this article was supported by European Research Fund for Coal and Steel. I would like to acknowledge the Polish Ministry of Science and Higher Education for the financing of the Polish part of this project. I would also like to thank the PGE GIEKSA Company for their help.

## References

- [1] Ang, A. H-S., Tang, W. H. 2007. Probability Concepts in Engineering. 2nd edit., Wiley & S Baecher, G. B., Christian, J. T. 2003. Reliability and Statistics in Geotechnical Engineering. Vilnius & Sons.
- [2] Bednarczyk, Z., 2018, Identification of flysch landslide triggers using nearly real-time monitoring data-an example from the Carpathian Mts., Poland. Engineering. Geology. 244, pp.41-56.
- [3] Bednarczyk, Z., 2017a, Slope Stability Analysis for the Design of a New Lignite Open-Pit Mine, Procedia Engineering, <https://doi.org/10.1016/j.proeng.2017.05.153>, V 190, pp. 51-58.
- [4] Bednarczyk, Z., 2017b, Landslide Monitoring and Counteraction Technologies in Polish Lignite Opencast Mines, Advancing Culture of Living with Landslides, Vol 5, Landslides in Different Environments edited by Matjaz Mikoz, Vít Vilfimek, Yueping Yin, Kyoji Sassa, Springer International, ISBN 978-3-319-53482-4, DOI 10.1007/978-3-319-53483-, pp 33-43.
- [5] Bednarczyk J., Nowak A., 2010, Strategie i scenariusze rozwoju produkcji energii elektrycznej z węgla brunatnego w obecnych warunkach (Strategies and scenarios for the future development of electricity production from lignite in the light of the existing conditions). Gornictwo i Geoinżynieria 34/4, pp. 67-83, [(in Polish)].
- [6] Bednarczyk, Z., Sandven R. 2004, Comparison of CPTU and laboratory tests interpretation of Polish and Norwegian clays, Fonseca V. (Editor) International Geotechnical and Geophysical Site Characterization Conference ISC-2 Porto, Millpress, pp. 1791-1799.
- [7] CEN (1994). EUROCODE 7, Geotechnical design.Part 1:Gen. rules,ENV1997-1E. Brussels.
- [8] Chowdhury, R. N., Nguyen, V. U. (1986). Spoil stability considering progressive failure. Min. Sci. Technology V3,127-139
- [9] Ciuk E. Piwocki M., 1980, Geologia trzeciorzędu Rowu Kleszczowa i jego otoczenia (Geology of the Tertiary in the Kleszczow Ditch and its surrounding area. In: Przewodnik LII Zjazdu PTG), pp. 38-56, [(in Polish)].
- [10] Cooper, M. A. 1987 Control Surveys in Civil Engin. William Collins Sons & Co., London. Christian, J. T., Ladd, C. C., 1994. Reliability applied to slope stability analysis. Jour. of Geot. Engin., 120 (12): 2180-2207.
- [11] Cooper, M. A. 1987 Control Surveys in Civil Engineering, William Collins Sons & Co. Ltd., London.
- [12] Cruden D. M., Varnes D., J., 1996, Landslide types and processes, In Turner AK, Schuster GP (eds.) Landslides, investigation and mitigation, Vol. 3. Special report 247, Transportation Res. Board, Nat. Res. Council National Acad. Press, Washington, pp. 36-75.
- [13] Demirel, N., Emil, M.K., Duzgun, H.S. 2011, Surface coal mine area monitoring using multi-temporal high-resolution satellite imagery. Inter. Journal of Coal Geology 86, pp. 3-11.
- [14] Demirel, N., Emil, M.K., Duzgun, H.S. 2011, Surface coal mine area monitoring using multi-temporal high-resolution satellite imagery. International Journal of Coal Geology 86, pp. 3-11
- [15] Dmitruk, S. 1984, Problems of geotechnical modeling in opencast mining, Wyd. Geol. 120 p.
- [16] Czarnecki L., Organisciak B. 2015, Zagrożenie utraty stateczności zbocza południowego zbudowanego ze skał mezozoicznych w obszarze rowu drugiego rzędu (Threat to the southern

- slope stability built of the Mesozoic bedrock, in the area of the sec-order ditch, In III Kongres Gorniczy C-5, [(in Polish)].
- [17] Czarniecki, L., Felisiak, I. 2004. Paleo-landslide block of the Southern Frame Fault and its influence on mining operations in the Second-order Graben at the Belchatow Lignite Mine. *Warszaty Gornicze Conf. Proc.* pp. 125 – 138. [(in Polish)].
- [18] Flisiak J., Rybicki S., Tylikowski, M. 2014 – Landslide risk assessment in Belchatow and Turow opencast mines. *Przeglad Geologiczny 10/2*: pp. 563-572, [(in Polish)].
- [19] Hawrysz, M., 2013, Metody szacowania efektywnych parametrów wytrzymałościowych (Methods of evaluation of soil strength effective parameters) *Geoinżynieria drogi mosty tunele Vol 3*, pp. 34-44, [(in Polish)].
- [20] Hochman A., 2000. Kopalnia Węgla Brunatnego Belchatów, od przedsiębiorstwa państwowego do spółki akcyjnej (Belchatow, mine from state enterprise to stock company) [(in Polish)].
- [21] Janecki W, Bednarczyk Z., Zembronski J., 1999 Rozpoznanie warunków geotechnicznych na zboczu południowym KWB Belchatow w rejonie zejścia do rowu drugiego rzędu na poziomie +124/+94 m n.p.m. w czwartym piętrze górnym pomiędzy liniami przekrojów 60 i 61 SN (Recognition of geotechnical conditions of the southern slope of the Belchatow mine in the area of the descent to the second order ditch and the northern slope at an altitude of +124/+94 a.s.l. in the 4th mining floor, between 60 and 61 SN lines), *Geosoft* [(in Polish)].
- [22] Jonczyk, W., Organisciak, B. 2010, Zagrożenia naturalne w KWB Belchatów rozpoznanie i przeciwdziałanie (Natural hazards in Belchatow Mine identification and counteraction), *Gornictwo i Geoinżynieria*, 34/4, pp. 249-257, [(in Polish)].
- [23] Kasztelewicz, Z. 2012, Węgiel brunatny w Polsce i na świecie (Brown coal in the world and in Poland), *Węgiel Brunatny Vol 78/1*, pp. 7-13, [(in Polish)].
- [24] Kossowski L., Olszewski B., Sowinski L., Wojturska M., Sowa J. 1992. Reinterpretacja budowy geologicznej KWB Belchatów pomiędzy liniami 42-70NS (Reinterpretation of geology of Belchatow lignite deposit in cross-sections 42-70NS). *Archiwum KWB Belchatow*, (in Polish).
- [25] Kulhawy, F. H. 1992. On the evaluation of static soil properties. In: *Geotechnical Special Publication 31: Stability and performance of slopes and embankments II*, ASCE. Berkeley, California, pp. 95-115.
- [26] Lu, D., Weng, Q., 2007. A survey of image classification methods and techniques for improving classification performance. *Intern. Jour. of Remote Sensing Vol. 28*, pp. 823–870.
- [27] Marinos, Vp., E Hoek, E., 2005, The Geological Strength Index: Applications and limitations. *Bull. Eng. Geol. Environ.* Vol. 64, pp. 55-65.
- [28] Nguyen, V. U., Chowdhury, R. N. 1984. The probabilistic study of spoil pile stability in strip coal mines - two techniques compared. *Int. J. Rock Mech. Min. Sci. Geom.* A.21 pp. 303-312.
- [29] Marshall, A., Rezanian, M., Heron, C., Marsh, S., Smith, M. Zanganeh, H., Masoudian, M., Hashemi, A., Bowman A., Fernández, A., Gullón, A., Rodrigo, C., De Cabo, M., Pozo, V., De Paz, D., Galera, J., Bednarczyk, Z., Svoboda, P., Burda, J., Koukouzas, N., Deliveris, A., Zevgolis, I., Coggan, J., Eyre, M., Vanneschi, M. Coccia, S., Cauvin, L., Al Heib, M. Richard, T. 2019 Draft Final Slopes Project Report Deliverable 4.3.1. European Commission Research Programme of the Research Fund for Coal and Steel, Technical Group: TGC1, Grant Agreement number RFCR-CT-2015-00001 Project Slopes - Smarter Lignite Open Pit Engineering Solutions: 1-120.
- [30] Marinos, Vp., E Hoek, E., 2005. The Geological Strength Index: applications and limitations. *Bull. Eng. Geol. Environ* 2005 64, pp. 55-65.
- [31] Patrzyk, J. 1996, Zagrożenie osuwiskowe w KWB Belchatów (Landslide threats in Belchatów Mine). *Mies. WUG*, 2/96 pp. 13–16, (in Polish).
- [32] Phoon, K., Kulhawy, F.H. 1999, Characterization of geotechnical variability, *Canadian. Geotechnical Journal*. Vol. 36, pp. 612–624.
- [33] PN EN 1997-1:2008 - Eurocode 7, Geotechnical design. Part 1: General principles (in Polish).
- [34] PN-EN 1997-2:2009- Eurocode 7, Geotechnical design. Part 2: Soil investigations [(in Polish)].
- [35] Poltegor-Projekt 2002 Aktualizacja projektu dla Pola Szczerców. Wydobycie maksymalne wraz z biznesplanem (Update of design project for Szczercow field for maximal exploitation together with the business plan), Wroclaw Nr projektu - 1030.1325.002. (in Polish).
- [36] Rybicki S. 1996, Osuwiska w Polskich kopalniach odkrywkowych węgla brunatnego (Landslide phenomena in Polish brown coal mines, In: *Geotechnical Problems in Engineering Practice*). Wyd. Polit. Krakowskiej: 157–164, [(in Polish)].
- [37] Schroeter, L., Gläßer, C., 2011, Analyses and monitoring of lignite mining lakes in East Germany with spectral signatures of Landsat TM. *Int. Jour. of Coal Geol.* Vol. 86, pp. 27-39.
- [38] Welsch, W., Heunecke, O., Kuhlmann, H., 2000, Auswertung geodätischer Überwachungsmessungen [In: Möser et al. (eds.): *Wichmann Verlag, Heidelberg, Wilkins*
- [39] Whitman, R. V. 1984. Evaluating calculated risk in geotechnical engineering. *Jour. of Geot. Engin.*, 110 (2): 143-188
- [40] Wilkins R., G. Bastin, And Chrzanowski A. 2003, ALERT: a fully automated real-time monitoring system. In: *Proc. of the 11th FIG Symposium on Deformation Measurements, Santorini, Greece*, pp 209-216.
- [41] Welsch, W., Heunecke, O., Kuhlmann, H., 2000, Auswertung geodätischer Überwachungsmessungen [Evaluation of geodetic monitoring measurements], In: Möser et al. (eds.): *Handbuch Ingenieurgeodäsie. Wichmann Verlag, Heidelberg*, (in German).
- [42] Wu, T. H. H., 2008. Reliability analysis of slopes. In: *Reliability-bas. Design in Geotechnics*.